Available online at www.sciencedirect.com
ScienceDirect
Acta Materialia 57 (2009) 6102–6112
Acta MATERIALIA
www.elsevier.com/locate/actamat

Misorientation texture development during grain growth. Part I: Simulation and experiment

J. Gruber *, H.M. Miller, T.D. Hoffmann, G.S. Rohrer, A.D. Rollett

Department of Materials Science and Engineering, Carnegie Mellon University, 5000 Forbes Avenue, Pittsburgh, PA 15213-3890, USA

Received 28 March 2009; received in revised form 15 August 2009; accepted 17 August 2009
Available online 5 October 2009

Abstract

Grain growth in two and three dimensions with anisotropic interfacial properties was simulated using the Monte Carlo method. The relative effects of grain boundary energy and mobility anisotropy on number- and area-weighted misorientation distribution functions (MDFs) were compared. Results indicate that energy anisotropy has a measurable effect on misorientation texture development, while mobility anisotropy does not. Qualitatively similar results are obtained in all simulations regardless of dimensionality or crystal symmetry. Microstructures with random orientation texture appear to evolve steady-state MDFs, while those with a preferred orientation do not. Experimentally measured number- and area-weighted MDFs in polycrystalline magnesia are shown to be comparable to those measured in our simulations.

Keywords: Texture; Grain growth; Anisotropy; Grain boundaries; Simulation

1. Introduction

Recent measurements of interfaces in polycrystalline ceramics and alloys have demonstrated that grain boundary character distributions (GBCDs) and misorientation distribution functions (MDFs) are often significantly nonrandom [1–10]. Additionally, a number of these reports suggest that thermomechanical processing can be used to control the relative frequency of internal interfaces with special properties [2,8–11]. These processes have been shown to result in improved bulk properties, e.g. corrosion resistance or ductility. The ability to predict and control interface texture is an essential step towards taking full advantage of this technology.

The question of how nonrandom distributions of internal interfaces develop has not yet been fully answered. Grain growth in a single-phase solid with anisotropic interfacial properties is perhaps the simplest physical process that might lead to interface texture, and several computational studies have reported the influence of anisotropic interfacial properties on interface texture development [12–20]. Results from these simulations suggest that grain growth with anisotropic interfacial energy can result in grain boundary distributions similar to those measured in real materials.

Misorientation texture can develop as a result of changes in the relative number of grain boundaries, the average area of grain boundaries, or both. However, most studies of misorientation texture development have focused only on changes to the area-weighted MDF. Previous simulation work has shown that grain boundaries with relatively low energy occur with greater than random frequency in area-weighted MDFs. In particular, Holm et al. [14] introduced a model for interface texture development that explains the observed changes in area-weighted MDFs by boundary lengthening at triple junctions. Although this model provides a physically reasonable mechanism for relative area change, it does not predict the experimentally observed texture in the number-weighted MDF. For example, Saylor

* Corresponding author. Tel.: +1 412 476 5282.
E-mail address: gruberja@gmail.com (J. Gruber).

1359-6454/$36.00
doi:10.1016/j.actamat.2009.08.036

et al. [6] have reported an increase in both the relative number and area of low-energy boundaries in polycrystalline strontium titanate.

In this work, we use conventional Monte Carlo simulations to re-examine the effect of interfacial anisotropy on misorientation texture development during grain growth. The influence of various anisotropic energy and mobility functions on MDFs are determined for a number of systems in both two and three dimensions. We provide simulated and experimental evidence that both area- and number-weighted MDFs are measurably affected by anisotropic interfacial properties. These results provide the motivation for a companion paper, hereafter called Part II, which presents an improved model for predicting misorientation texture development during grain growth [21].

2. Simulations

2.1. Microstructure generation

Because we do not expect grain boundaries with relatively few pixels or voxels to accurately reproduce curvature driven grain growth, we begin each simulation with a microstructure that has a relatively large average number of lattice sites per grain. We use either a 4096^2 square (two-dimensional, 2-D) or 256^3 cubic (three dimensional, 3-D) lattice. To produce the initial microstructure, unique spin numbers were assigned to each lattice point, and the microstructure was coarsened with isotropic interfacial properties. After coarsening, the grains and grain boundaries are reasonably well resolved, with an average of approximately 244 (2-D) or 470 (3-D) lattice sites per grain. The initial 2-D microstructure had 68,651 grains and 203,271 grain boundaries, while the 3-D microstructure had 35,751 grains and 238,412 grain boundaries.

Each spin number in the Monte Carlo lattice is mapped to a unique crystallographic orientation. To produce a random orientation texture, we generate (Bunge convention) Euler angles [22]

$$\begin{aligned} \varphi_1 &= 2\pi r_1 \\ \Phi &= \cos^{-1}(1-2r_2) \\ \varphi_2 &= 2\pi r_3 \end{aligned} \tag{1}$$

where each r_i is a random floating point number in the interval $0 \leqslant r_i \leqslant 1$. We also use nonrandom orientation assignments to investigate the effect of texture. In this case, orientations are generated randomly as above, but are selected with a probability P based on their proximity to a single favored orientation coinciding with a reference orientation. Without loss of generality, we choose the sample coordinate system. With the disorientation angle from the sample axes ϑ, we set

$$P(\vartheta) = e^{-\alpha\vartheta} \tag{2}$$

where α is a constant. The value $\alpha = 0$ corresponds to random orientation texture, while larger values of α produce orientation textures that increasingly favor the preferred orientation. Note that, regardless of the dimension of the simulation domain, our orientations are completely general 3-D rotations.

In this work, the time evolution of any grain boundary depends on both its local geometry and its misorientation-dependent properties. By performing simulations with different spin to orientation mappings, we can effectively sample many sets of grain boundaries without generating additional microstructures. For each set of interfacial properties we use 20 such mappings, sampling more than four million grain boundaries at the initial state.

2.2. Monte Carlo method

The formulation of the Monte Carlo method used here is based largely on common practice (see e.g. [23]). The total system energy is given by

$$E = E_0 + \sum_{i=1}^{N}\sum_{j=1}^{N}\gamma(\theta_{ij})\chi(i,j) \tag{3}$$

where E_0 is the reference state energy, N is the number of lattice sites, $\gamma(\theta_{ij})$ is the energy per unit area of grain boundary with disorientation angle θ_{ij}, and $\chi(i,j)$ is a function that is one if site i is a near neighbor of site j and zero otherwise. Thus the only driving force for grain boundary motion is the reduction of interfacial energy. For a general lattice site, we use the 8 (2-D) or 26 (3-D) nearest lattice sites as neighbors. These correspond to first and second nearest neighbors on a 2-D square lattice or first, second and third nearest neighbors on a 3-D cubic lattice. Finite boundary conditions are imposed, and therefore sites on the domain boundary have fewer neighbors than interior sites.

The microstructure is evolved by an algorithm that allows any site chosen at random to switch spins to that of a nearest neighbor. Here we choose a possible new spin randomly from a list of neighbor spins, although our tests with alternative algorithms, such as that of Ono et al. [13], produce similar results. We use the convention that N (number of lattice sites) such possible flips constitute one Monte Carlo step (MCS). A spin flip occurs with a probability P that depends on the total energy change of the system ΔE, as well as grain boundary energy and mobility:

$$P = \begin{cases} \frac{M(\theta_{ij})}{M_{\max}}\frac{\gamma(\theta_{ij})}{\gamma_{\max}} & \Delta E \leqslant 0 \\ \frac{M(\theta_{ij})}{M_{\max}}\frac{\gamma(\theta_{ij})}{\gamma_{\max}}\exp\left[-\frac{\Delta E}{\beta\gamma(\theta_{ij})}\right] & \Delta E > 0 \end{cases} \tag{4}$$

ΔE is calculated by evaluating Eq. (3) for both the altered state and the original state, then computing their difference. The constants $\gamma_{\max}$ and $M_{\max}$ are the maximum allowed grain boundary energy and mobility, respectively. We use $\gamma_{\max} = 1$ and $M_{\max} = 1$ in all simulations. The constant β is an effective "lattice temperature". For 2-D simulations we set $\beta = 0.7$, while for 3-D simulations $\beta = 1.5$.

Several choices made here, while common, are only a matter of preference when performing Monte Carlo simulations. For example, we perform simulations on Cartesian grids, although other discretizations, such as the triangular lattice (2-D), are common. Likewise, periodic boundary conditions are often used as an alternative to finite boundary conditions. Although these choices generally have little effect on the microstructural evolution, it is known that choosing an inappropriate value of β can lead to effects such as lattice pinning (low β) or disordering (high β). We have demonstrated elsewhere [24] that the relevant data we wish to extract from Monte Carlo simulations are insensitive to the boundary conditions used or to our choice of lattice temperature β.

2.3. Interfacial properties

Although a general misorientation is characterized by three independent parameters, the grain boundary properties used in this work are explicit functions of a single parameter, the grain boundary disorientation. The disorientation is defined as the smallest rotation angle from all symmetrically equivalent misorientations. Our choice of interfacial energy and mobility are therefore not completely general functions of misorientation. However, our results should be largely applicable to such cases, as will be discussed in Part II.

A number of grain boundary properties were used in simulations with random initial orientation texture. The grain boundary energy and mobility functions used here are based on the Read–Shockley function [25]

$$\gamma_{\mathrm{RS}}(\theta) = \begin{cases} \frac{\theta}{\theta'}\left[1 - \ln\left(\frac{\theta}{\theta'}\right)\right] & \theta \leqslant \theta' \\ 1 & \theta > \theta' \end{cases} \tag{5}$$

where θ is the grain boundary disorientation angle and θ' is the constant cutoff angle, or a step function defined by

$$\gamma_{\mathrm{step}}(\theta) = \begin{cases} \frac{3}{5} & \theta \leqslant \theta' \\ 1 & \theta > \theta'. \end{cases} \tag{6}$$

where, again, θ is the disorientation angle. Note that such functions incorporate crystallographic symmetry implicitly in the computation of disorientation angles. The same energy functions are used in both 2-D and 3-D simulations (recall that in both cases fully 3-D orientations are mapped to spins). We perform simulations with cubic crystal symmetry and the Read–Shockley function, $\theta' = 0°, 15°, 30°$, and 45°, as done in previous 2-D work by Holm et al. [14], albeit at a different lattice temperature and with a triangular lattice. Note that $\theta' = 0°$ implies isotropy. We also include simulations with hexagonal crystal symmetry and the Read–Shockley function with $\theta' = 45°$ to determine what effect crystal symmetry has on interface texture development. While the Read–Shockley functions are physically motivated, the step function is used to illustrate several concepts that are discussed more completely in Part II. Finally, simulations with mobility anisotropy in the form of the Read–Shockley function were used for comparing the relative effects of mobility anisotropy on misorientation texture to those of energy anisotropy. In this case,

$$M_{\mathrm{RS}}(\theta) = \begin{cases} \frac{\theta}{\theta'}\left[1 - \ln\left(\frac{\theta}{\theta'}\right)\right] & \theta \leqslant \theta' \\ 1 & \theta > \theta' \end{cases} \tag{7}$$

with $\theta' = 45°$, while the energy function is chosen to be isotropic, i.e. $\gamma(\theta) = 1$.

Additionally, several 3-D simulations were performed with anisotropic energy, cubic crystal symmetry and nonrandom initial orientation distributions. Using the probability function defined by Eq. (2), we chose $\alpha = 4.20, 6.05, 9.45$, or 16.80. These values of α result in initial (cubic) MDFs that are essentially zero for disorientations above 60°, 50°, 40° and 30°, respectively. All simulations with nonrandom initial orientation texture were performed using the 3-D microstructure with $\gamma_{\mathrm{RS}}, \theta' = 45°$ and isotropic mobility. Here, as in all 3-D simulations, we use $\beta = 1.5$ and finite boundary conditions.

2.4. Analysis

Measuring geometric features of a microstructure that depend on crystallographic orientation requires a choice in what constitutes a single grain or grain boundary. In experiments, the limited accuracy of orientation measurement imposes a lower bound for grain boundary misorientation. This is not the case with Monte Carlo simulations. Since each lattice point has a discrete spin or grain number that is associated with a fixed orientation, the misorientation resolution limit is due only to numerical truncation error, which is negligible. In our simulations we occasionally observe two or more "grains" of low misorientation meeting together, which then evolve as essentially a single grain. We have chosen to impose a minimum disorientation angle of 2° in all or our analysis so that our simulations are more directly comparable to experiment.

Likewise, a suitable definition of grain boundary area on a discrete lattice is required for the measurement of area-weighted misorientation distribution functions. Since the method used in evolving the system weights all nearest neighbors of a lattice point equally, we have chosen to count each pair of neighboring sites with different spins as a unit grain boundary area. Although not presented here, area-weighted MDFs were also computed using only 4 (2-D) or 6 (3-D) nearest neighbors. There were no significant differences between area-weighted MDFs computed using either method. While other neighbor counting schemes may compute different absolute areas for a given boundary, we assume that relative area measurements are insensitive to the neighbor counting method since these two neighbor counting schemes effectively compute upper and lower bounds for the absolute area measurement.

Measuring number-weighted MDFs involves the same procedure used in the area measurement, but individual grain boundaries are given unit weight. To simplify this

calculation, we assume that, if two grains share a boundary, they share a single boundary. Therefore the set of all neighbor pairs with spins i and j contribute one grain boundary to the number count, while contributing a value equal to the total number of such pairs to the area measurement.

Because grain boundaries are continuously eliminated throughout grain growth, it becomes increasingly difficult to measure MDFs with a fixed angular resolution as each simulation progresses. Additionally, random orientation texture creates a bias for high angle grain boundaries around the 45° disorientation. This implies that collecting statistical data for low angle boundaries requires a significantly larger sample of other boundary types. Given the number of grains in our initial microstructures, we find that the area- and number-weighted MDFs can be measured accurately with a 2° resolution in disorientation angle only until the average grain diameter has increased approximately fourfold.

3. Experiment

3.1. Sample preparation

A polycrystalline, 3000 ppm Ca-doped MgO sample was prepared for electron backscatter diffraction (EBSD) mapping. High-purity carbonates (Alfa Aesar Puratronic $MgCO_3Mg(OH)_2 + XH_2O$ 99.996%, Alfa Aesar Puratronic $CaCO_3$ 99.999%) were dry-ground in an alumina mortar to promote mechanical mixing and uniform distribution of the dopant. The combined carbonates were then calcined at 1100 °C for 5 h in three nested MgO crucibles to avoid contamination in the furnace. The resultant powder was again dry-ground and then compacted to approximately 1000 psi in a half inch diameter cylindrical die using a Carver uniaxial press. The pellet was placed on a bed of mother powder in three nested MgO crucibles and fired using the program: 5 °C min^{-1} to 900 °C for 10 h, 5 °C min^{-1} to 1200 °C for 7 h, 5 °C min^{-1} to 1600 °C for 7 h, 5 °C min^{-1} to room temperature. Rough grinding was completed with progressively finer SiC paper, using Buehler Metadi fluid as a lubricant as water tends to degrade MgO specimens. Final polishing was accomplished using 1 μm and 0.1 μm diamond in oil on Buehler Mastertex cloth. The sample was then annealed at 1200 °C for 2 h and carbon coated (SPI-Module Carbon Coater) to eliminate charging under the electron beam.

3.2. Data collection and analysis

Crystal orientation maps were obtained from a planar section using an EBSD mapping system (EDAX/TSL OIM, version 4.5) integrated with a scanning electron microscope (Philips XL40 FEGSEM). Maps were collected on a hexagonal grid with 1 μm spacing. In total, 20 scans were collected, covering a total area of 18.84 mm^2. In this sample, the average grain diameter was approximately 20 μm. Minimal processing of the data included "grain dilation clean-up" in the OIM software and assigning of an average orientation to each grain. Remaining single pixel grains and boundaries on such grains were ignored in the final analysis. The data were then sampled on a square grid and MDFs were computed with the same algorithm as used for the simulated data, as described above. The dataset used in computing the MDFs included 36,223 grains and 99,420 grain boundaries.

4. Results

4.1. General observations

The time-dependent behavior of grain size in simulations with anisotropic interfacial properties is approximately the same as that in isotropic growth, as shown in Fig. 1. The kinetic exponent n for isotropic growth in 3-D is found to be $n = 1.49$, which is near the theoretical volume rate of change exponent value of 1.5 [26]. This is nearly identical to the exponent for growth with anisotropic energy in all cases. The kinetic exponent for average grain area vs. time for isotropic growth in 2-D is found to be $n = 0.98$, again near the theoretical area rate of change value of 1.0. It is also clear that the absolute rate of grain growth for simulations with anisotropy is slower than with isotropic properties. Presumably, the rate is slower with anisotropy because the average energy or mobility of boundaries in such cases is less than it is in the isotropic case.

The grain size distribution in all simulations appears to be identical to that in the isotropic case (Fig. 2). Note that in our computations we have excluded grains comprising less than 10 lattice sites. We also observe that the grain size distribution does not change appreciably with time.

The grain morphology after 3-D growth with anisotropic properties is illustrated in Fig. 3. Grain shapes appear to be mostly equiaxed, and we can visually locate

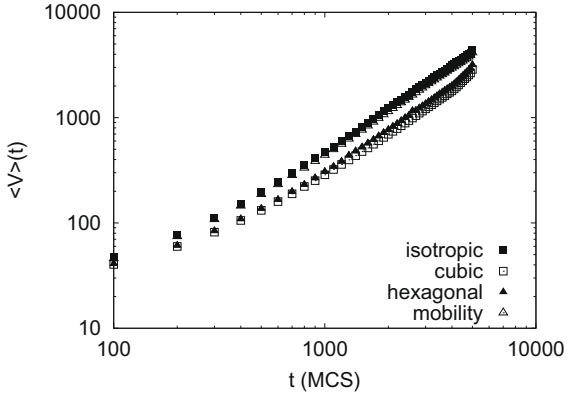

Fig. 1. Grain volume V as a function of time t for 3-D Monte Carlo simulations. Here, "cubic" and "hexagonal" imply $\gamma_{RS}(\theta)$ with $\theta' = 45°$ and isotropic mobility and cubic or hexagonal crystal symmetry, while "mobility" signifies $M_{RS}(\theta)$ with $\theta' = 45°$ and isotropic energy.

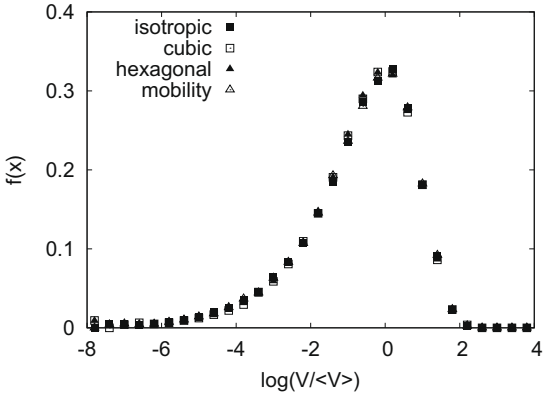

(a) Grain size distribution at 500 MCS.

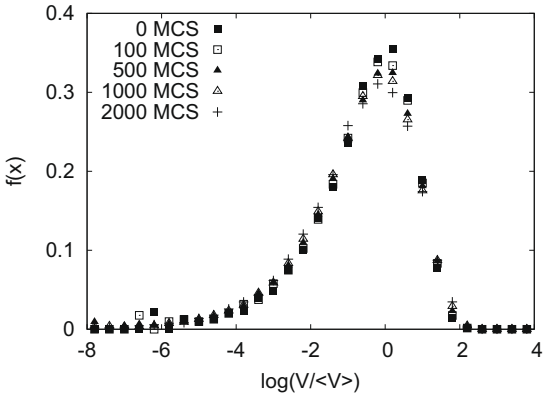

(b) Grain size distributions throughout simulation with γ_{RS}, $\theta' = 45°$.

Fig. 2. Grain size distributions for various 3-D Monte Carlo simulations.

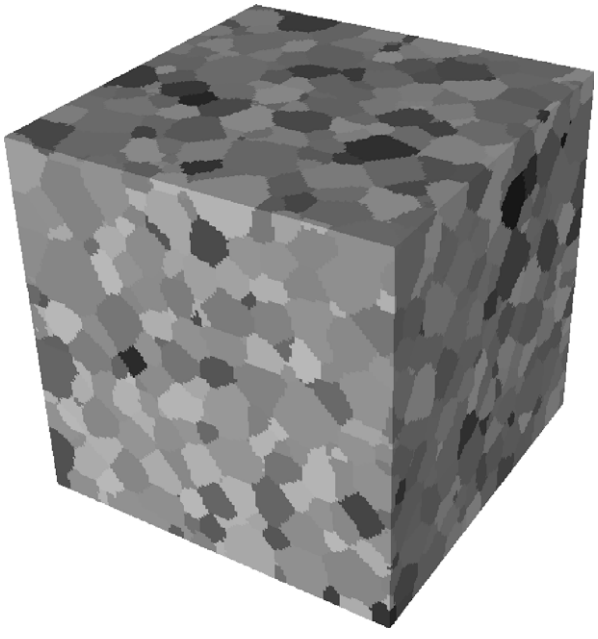

Fig. 3. Microstructure from grain growth with $\gamma_{RS}, \theta' = 45°$, 2000 MCS. One-eighth of the simulation domain is shown.

several triple junctions with apparent dihedral angles which are greater or less than the isotropic equilibrium value of 120°. The average topological properties of grains are roughly the same with or without anisotropy. Excluding grains on the domain boundary, we find that grains in three dimensions have an average of about 13.8 faces and 5.3 edges, while grains in two dimensions have 6.0 faces. These values remain approximately constant through time, and are similar to values reported elsewhere [27].

4.2. Time dependence

In simulations performed with random orientation distributions, we find that after an initial transient state, both area- and number-weighted MDFs reach what appear to be steady-state distributions. To quantify the transient, we introduce a value $\Delta(t)$, defined as

$$\Delta(t) = \int |f(\theta, t) - f(\theta, 0)|\, d\theta \tag{8}$$

where $f(\theta, t)$ represents either an area or number-weighted MDF depending on the context. Thus $\Delta(t)$ is just the L^1 norm of the difference between a pair of distributions, one of which is always the initial MDF. Note that $\Delta(t)$

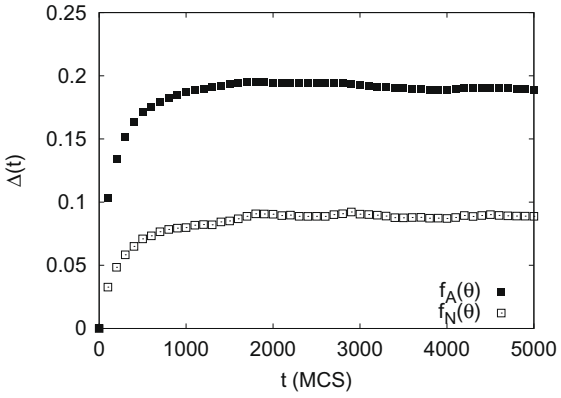

(a) Cubic crystal symmetry.

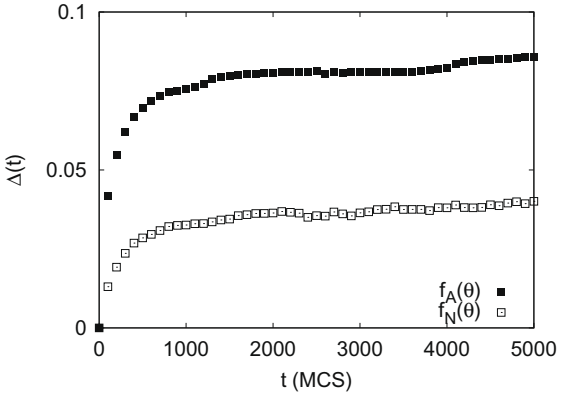

(b) Hexagonal crystal symmetry.

Fig. 4. Plots of $\Delta(t)$ for select 3-D Monte Carlo simulations with energy functions $\gamma_{RS}(\theta), \theta' = 45°$ and isotropic mobility.

approaching a constant as t increases is a necessary condition for the function $f(\theta, t)$ to reach a steady state.

In Fig. 4 we show the time dependence of $\Delta(t)$ for the area- and number-weighted MDF during two particular simulations. It is clear that for the simulation with cubic crystal symmetry, $\Delta(t)$ approaches some constant value. In other simulations and at long times $\Delta(t)$ continues to change slowly, although this change is on the order of $\Delta(t)$ for isotropy. This implies that further changes in the MDFs are due primarily to increasing measurement inaccuracy, as the total number of boundary observations decreases rapidly as grain growth progresses. We observe that the transient regime is consistently longer for simulations with larger energy anisotropy.

4.3. Property dependence

We observe a measurable change in the number- and area-weighted MDFs produced during grain growth with anisotropic interfacial energy. This is true for each energy function used and regardless of dimension. Figs. 5 and 6 show the steady-state number- and area-weighted MDFs for the simulations with cubic or hexagonal crystal symmetry and Read–Shockley energy functions with a 45° cutoff angle after a significant portion of the original grains have been eliminated by grain growth. In each case, the lowest-energy boundaries are those closest to the origin. These boundaries have increased in both number and average area relative to the higher-energy boundaries at larger disorientation angles. One consequence is that the area-weighted MDF in all cases shows greater anisotropy than the number-weighted MDF.

There appears to be a consistent inverse proportionality between the grain boundary energy and the average boundary area, as shown in Fig. 7. Fig. 7 also demonstrates that the relationship between grain boundary energy and average area may not always be one-to-one. This implies that the grain boundary's position in disorientation space has some influence on the average boundary area.

The effect of increasing energy anisotropy on the area- and number-weighted MDFs is illustrated in Fig. 8. We find that increasing energy anisotropy leads to both area- and number-weighted MDFs, which are increasingly different in comparison to those produced by isotropic grain growth. Fig. 9 shows the results of the simulations with energy anisotropy and isotropic mobility (labeled "energy"), and with anisotropic mobility and isotropic energy (labeled "mobility"). The effect of mobility anisotropy on the MDF is noticeably weaker than that of energy anisotropy. In fact, both area- and number-

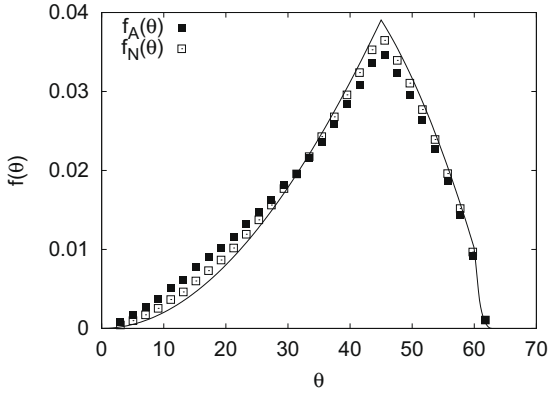

(a) Cubic crystal symmetry.

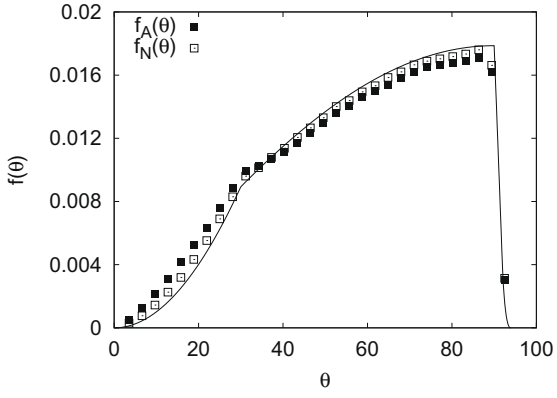

(b) Hexagonal crystal symmetry.

Fig. 5. Misorientation distribution functions after 2-D grain growth with energy functions $\gamma_{RS}(\theta), \theta' = 45°$ and isotropic mobility at 1000 MCS. In each case, the average grain area has doubled.

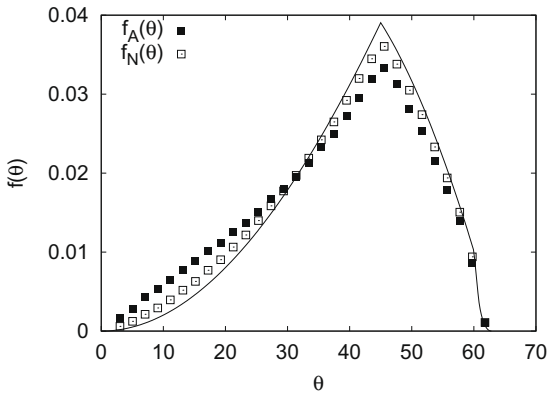

(a) Cubic crystal symmetry.

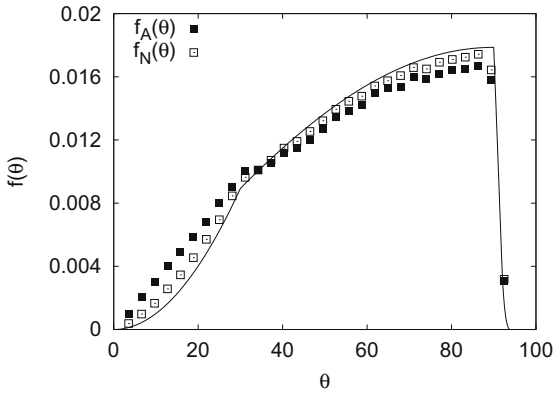

(b) Hexagonal crystal symmetry.

Fig. 6. Misorientation distribution functions after 3-D grain growth with energy functions $\gamma_{RS}(\theta), \theta' = 45°$ and isotropic mobility at 500 MCS. In each case, the average grain volume has doubled.

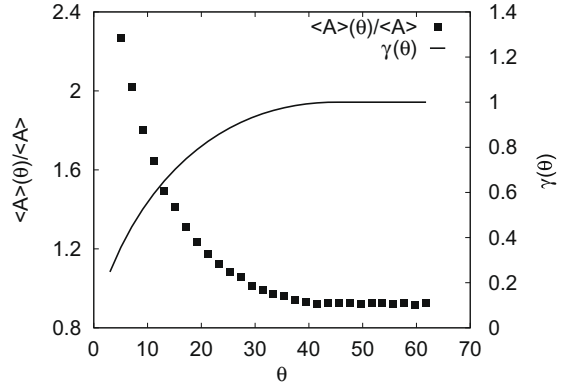

(a) $\gamma_{RS}(\theta)$, $\theta' = 45°$.

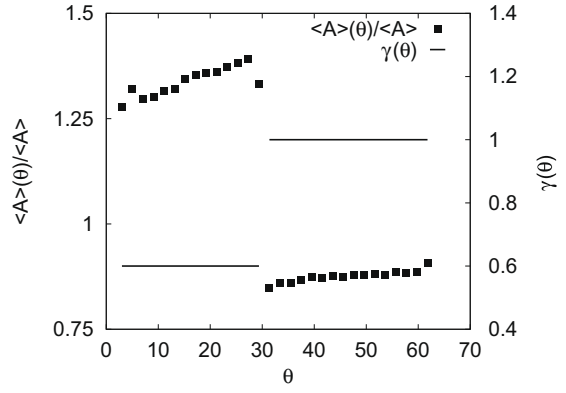

(b) $\gamma_{step}(\theta)$, $\theta' = 30°$.

Fig. 7. Normalized average boundary area $\langle A\rangle(\theta)/\langle A\rangle$ and grain boundary energy γ as a function of disorientation θ for Monte Carlo simulations with anisotropic energy, isotropic mobility and cubic crystal symmetry at 500 MCS.

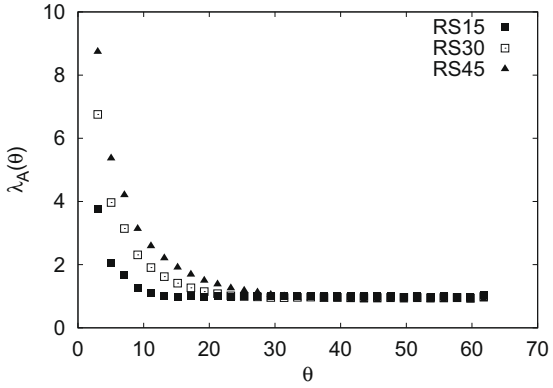

(a) Area weighted MDFs in multiples of random distribution (MRD).

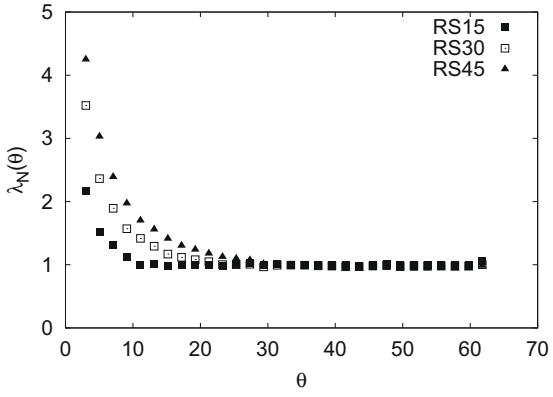

(b) Number weighted MDFs in multiples of random distribution (MRD).

Fig. 8. Area- and number-weighted MDFs in multiples random for various Read–Shockley-type energy functions and isotropic mobility. Data are from 3-D Monte Carlo simulations at 500 MCS.

weighted MDFs resulting from grain growth with mobility anisotropy are negligibly different from those developed with isotropic properties. These results are in agreement with previous findings using, for example, phase field and moving finite element methods [15,20].

4.4. Orientation texture dependence

The area- and number-weighted MDFs presented above for simulations with anisotropic energy all show deviations from a random distribution. Clearly, the orientation texture of the microstructure has a large effect in determining how the MDFs might evolve. We now describe results from simulations with nonrandom orientation texture.

First, we find that the kinetics of such simulations are not significantly different from the cases with random orientation texture. Fig. 10 shows the average grain volume (in voxels) as a function of simulation time. As above, the grain growth exponent in simulations with anisotropic energy tends to be slightly lower than with isotropy. Likewise, the grain size distribution appears to be similar for all simulation conditions as well as constant through time (Fig. 11).

The average area of grain boundaries in simulations with nonrandom orientation texture follows the same behavior as with random orientation texture (Fig. 12). These functions appear to be identical, but each shifted along the y-axis, likely due to the fact that those simulations with greater orientation texture have far fewer high-angle boundaries and therefore larger values of $\langle A\rangle$ at earlier simulation times.

Despite these similarities to simulations with random initial orientation texture, we find qualitatively different behavior of the area- and number-weighted MDFs. In particular, there appears to be no steady state within the time interval simulated (Fig. 13). Even in the most weakly textured case with $\alpha = 4.20$, where the initial MDFs do not appear to be particularly far from the Mackenzie distribution, the misorientation texture continues to evolve through time. As the average boundary areas are similar to those found with random orientation texture, it must be that this difference is due to a drastic increase in the number of low angle grain boundaries. We cannot exclude the possibility that these MDFs eventually reach a steady state without simulating to longer times.

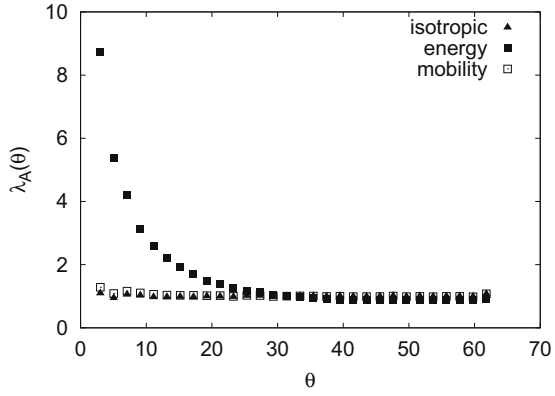

(a) Area weighted MDFs in multiples of random distribution (MRD).

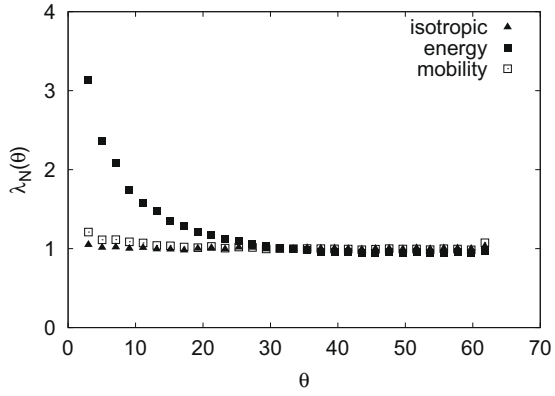

(b) Number weighted MDFs in multiples of random distribution (MRD).

Fig. 9. Area- and number-weighted MDFs for Read–Shockley-type energy or mobility functions. Data are from 3-D Monte Carlo simulations at 500 MCS.

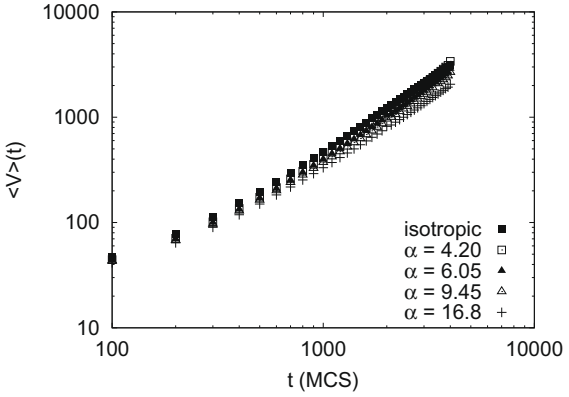

Fig. 10. Average grain volume $\langle V \rangle$ as a function of time for simulations with nonrandom orientation texture.

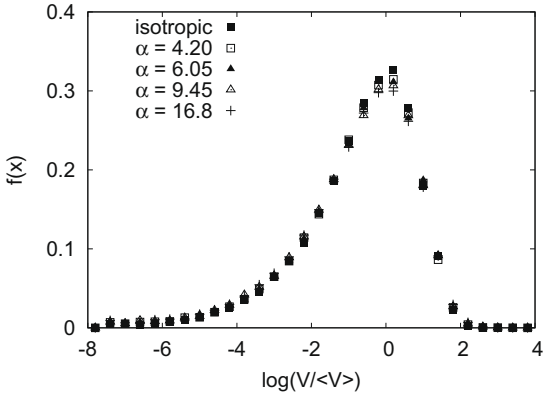

Fig. 11. Grain size distribution for simulations with nonrandom orientation texture at 500 MCS.

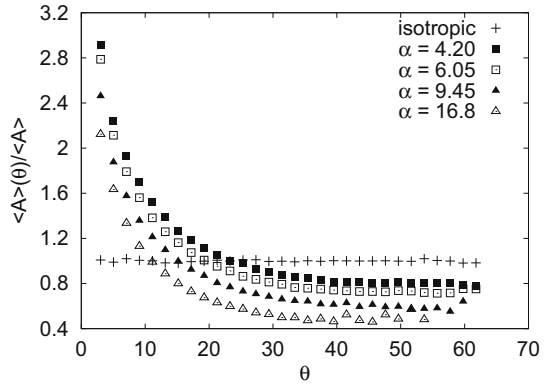

Fig. 12. Relative average area $\langle A \rangle(\theta)/\langle A \rangle$ of grain boundaries as a function of disorientation angle θ for simulations with nonrandom orientation texture at 500 MCS.

The reason for this increase in misorientation texture seems to be a the continuous strengthening of the orientation texture. Fig. 14 shows orientation distribution functions measured at the initial state and at 4000 MCS for the simulation with $\alpha = 4.20$. The initial orientation distribution shows preferential alignment with sample axes, as expected, while the orientation distribution at 4000 MCS shows that this preferred texture has become stronger as grain growth has progressed. Because we have chosen to use an energy function that is an increasing function of disorientation, we might expect that with our chosen orientation texture the high-energy boundaries typically exist on those grains that are not aligned with the sample axes. That is, we expect a correlation between high-energy grain boundaries and grains that do not have the preferred orientation. We have shown that high-energy boundaries are eliminated preferentially by the grain growth process, and presumably this affects the lifetime of such grains. In simulations with random orientation texture, there should be no correlation between high-energy boundaries and any grain orientation, explaining why there is no orientation texture development in such cases.

The orientation texture of the microstructure determines in some part what the expected MDFs should be. We define the texture-weighted MDF (TMDF) as the probability density of grain boundary types given by random selection of grain pairs from the polycrystal orientation distribution function (ODF). For example, in systems with

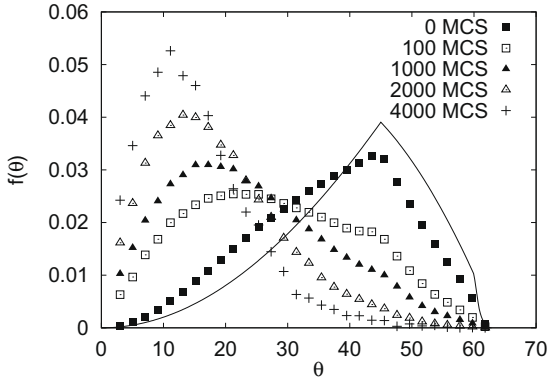

(a) Simulation with $\alpha = 4.20$.

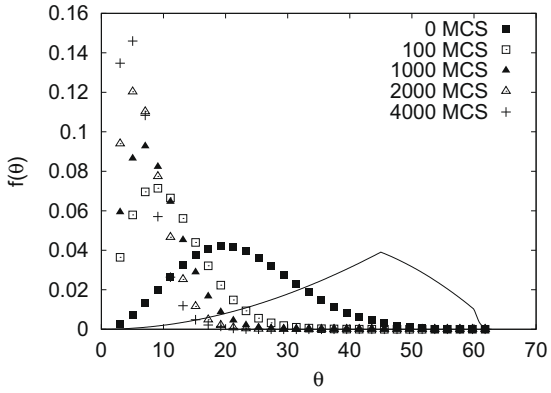

(b) Simulation with $\alpha = 16.80$.

Fig. 13. Area-weighted MDFs measured for simulations with nonrandom orientation texture.

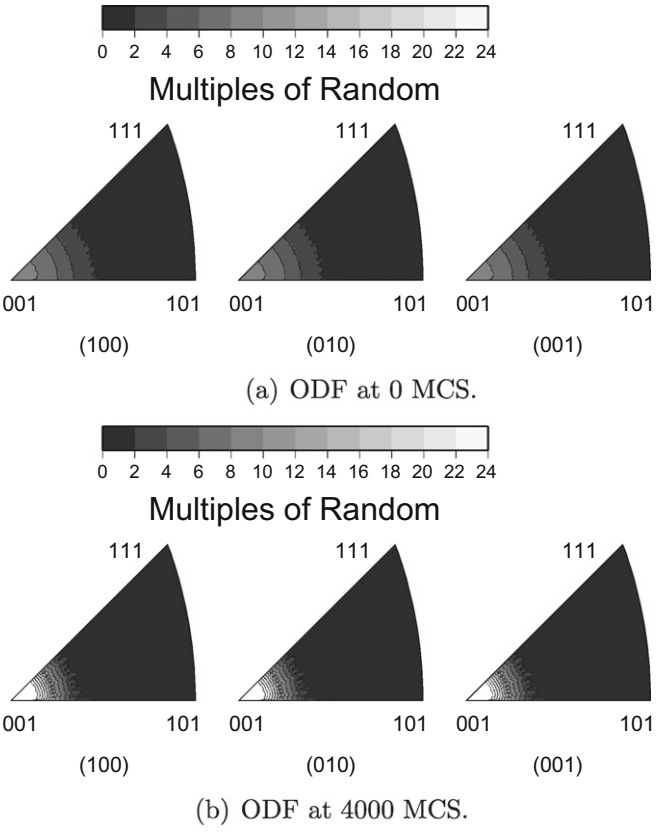

(a) ODF at 0 MCS.

(b) ODF at 4000 MCS.

Fig. 14. Orientation distribution function for simulation with nonrandom initial orientation texture with $\alpha = 4.20$ at 0 and 4000 MCS.

random orientation texture the TMDF is just the (cubic) Mackenzie distribution or its analogue for other crystal symmetries. The TMDF can be estimated numerically from orientation texture data by randomly selecting existing pairs of grain orientations, thereby generating a list of possible grain boundaries with which to compute the TMDF in the same way that we compute the MDF. Fig. 15 shows the texture weighted MDF as a function of time for two simulations with nonrandom orientation texture. The changing orientation texture increases the bias towards low angle grain boundaries, and this appears to be the primary reason for the differences between the MDFs measured in these and the random orientation texture simulations.

4.5. Validation of simulation results

Here we compare our results with experimental measurements from polycrystalline magnesia samples with random orientation texture. The experimentally measured MDFs from polycrystalline MgO exhibit the same trends as our simulations, as shown in Fig. 16. Both number- and area-weighted MDFs are measurably nonrandom, with low-angle boundary enhancement comparable to the simulation with $\gamma_{RS}, \theta' = 15^\circ$. Significant deviations occur in the two low-angle bins, presumably due to an insufficient total number of observations (15 and 41 observations, respectively). While the absolute changes in the number- and area-weighted MDFs are similar, it is clear that the average area of low-angle boundaries has increased, as in Fig. 16. These results suggest that an increase in both the number and average area of grain boundaries contributes to interface texture development in real materials.

5. Discussion

As previously stated, the fact that the area fraction of low-energy grain boundaries increases during grain growth has been observed in a number of 2-D and 3-D simulations [12–14,16,20]. There are inherent difficulties in measuring the number-weighted MDF for the low-angle regime in microstructures with random orientation texture, as the proportion of such boundaries is only a small fraction of the total number of grain boundaries. While nearly all of the listed studies lack measurements of the number-weighted MDF, we note that Holm et al. [14] report a "minimal increase" in the number-weighted MDF during anisotropic growth. Although they do not report the number of boundaries used in computing MDFs, from inspection of their microstructure at the time of computation, and assuming three boundaries per grain, a reasonable approximation is 3750 grain boundaries. We find that the

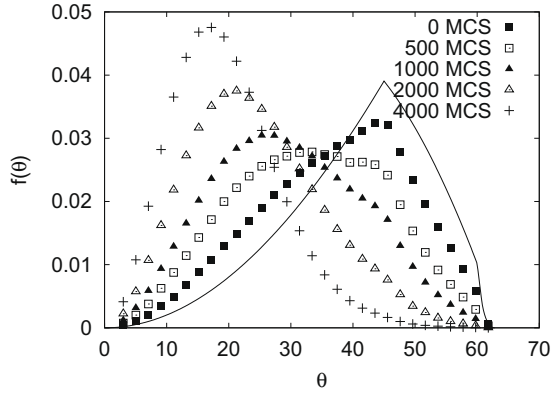

(a) Simulation with $\alpha = 4.20$.

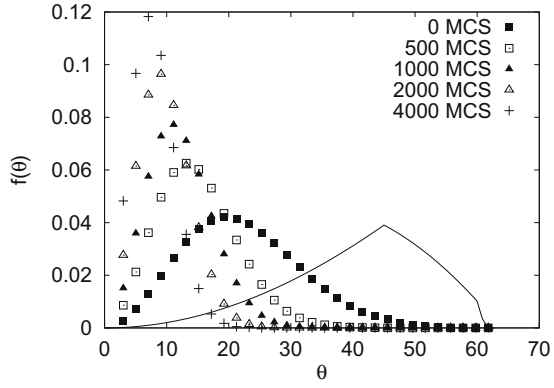

(b) Simulation with $\alpha = 16.80$.

Fig. 15. TMDF as a function of time for simulations with nonrandom orientation texture.

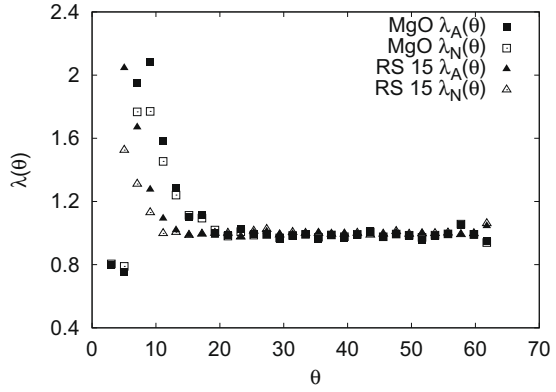

(a) Area and number weighted MDFs in multiples random distribution.

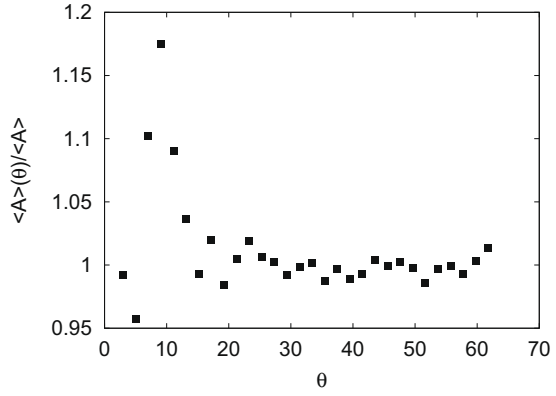

(b) Relative average grain boundary area.

Fig. 16. Area- and number-weighted MDFs and relative average grain boundary area from polycrystalline magnesia with random orientation texture.

number-weighted MDF appears random in measurements with fewer than 10,000 grain boundaries. Presumably, the small increase in the number-weighted MDF for low-energy boundaries was comparable to the noise in their measurements. Because we have found a measurable anisotropy in the number-weighted MDF of a real material (Fig. 16) which is quantitatively similar to those found in our simulations, we conclude that changes in both the relative number and area of grain boundaries occur during grain growth.

Holm et al. [14] proposed a model for the increased length (area) of low-energy boundaries driven by the requirement of interfacial equilibrium at triple junctions. This model attempts to explain why low-energy grain boundaries have relatively larger average areas, which the present study (Fig. 7) and others have confirmed [20]. Such a model, however, does not explain why low-energy boundaries also appear in greater numbers. Because the number of boundaries of any type changes only by topological events that create or annihilate grain faces within the boundary network, a suitable model must depend in some way on the relative rates of such events. A model based on these rates will be presented in Part II [21].

The grain boundary energy anisotropy has a much larger influence on interface texture development than mobility, which is in agreement with previous findings [15,20]. All such computations were performed on simulation domains with random orientation texture, and it is likely that given a nonrandom initial orientation texture, mobility anisotropy might contribute to changes in the MDF, e.g. as in abnormal growth [28,29]. Here we have only studied the effect of energy anisotropy on grain growth in systems with nonrandom orientation texture, but our results are qualitatively similar to previous work with stronger texture [14].

Finally, we note that misorientation texture development occurs without any significant effect on such microstructural features as the grain size distribution, average grain properties like the number of edges or faces, and only a minimal change in grain growth rate.

6. Conclusions

Monte Carlo simulations of 2-D and 3-D grain growth with anisotropic energy and mobility and random orientation texture were performed. Grain boundary energy anisotropy was found to produce a measurable effect on both number- and area-weighted MDFs. The average area

and number of relatively low-energy grain boundaries increases relative to higher-energy grain boundaries. The effect of mobility anisotropy on interface texture appears to be insignificant, in agreement with previous results. In simulations with random orientation texture, both area-weighted and number-weighted MDFs develop into steady-state distributions after some initial transient, while simulations with a preferred orientation texture exhibit a continuously evolving MDF. Similar results are obtained in all simulations regardless of dimensionality, crystal symmetry or the form of the energy function. Measured number- and area-weighted MDFs in polycrystalline MgO are qualitatively similar to those produced by simulations with anisotropic energy.

Acknowledgements

This work was supported by the MRSEC program of the National Science Foundation under award number DMR-0520425 and by the Computational Materials Science Network program of the Office of Basic Energy Sciences, Department of Energy. J.G. wishes to acknowledge the helpful suggestions provided by E.A. Holm.

References

[1] Saylor DM, Morawiec A, Rohrer GS. J Am Ceram Soc 2002;85(12):3081–3.
[2] Randle V, Davies H. Metall Mater Trans A 2002;33(6):1853–7.
[3] Saylor DM, Morawiec A, Rohrer GS. Acta Mater 2003;51(13):3663–74.
[4] Rohrer GS, Saylor DM, El Dasher B, Adams BL, Rollett AD, Wynblatt P. Z Metallkd 2004;95(4):197–214.
[5] Saylor DM, El Dasher BS, Rollett AD, Rohrer GS. Acta Mater 2004;52(12):3649–55.
[6] Saylor DM, El Dasher B, Sano T, Rohrer GS. J Am Ceram Soc 2004;87(4):670–6.
[7] Saylor DM, El Dasher B, Pang Y, Miller HM, Wynblatt P, Rollett AD, et al. J Am Ceram Soc 2004;87(4):724–6.
[8] Kim CS, Hu Y, Rohrer GS, Randle V. Scripta Mater 2005;52(7):633–7.
[9] Randle V, Hu Y, Rohrer GS, Kim CS. Mater Sci Technol 2005;21(11):1287–92.
[10] Rohrer GS, Randle V, Kim CS, Hu Y. Acta Mater 2006;54(17):4489–502.
[11] Miller HM, Kim C-S, Gruber J, Randle V, Rohrer GS. Mater Sci Forum 2007;558-559:641–7.
[12] Hinz DC, Szpunar JA. Phys Rev B 1995;52(14):9900–9.
[13] Ono N, Kimura K, Watanabe T. Acta Mater 1999;47(3):1007–17.
[14] Holm EA, Hassold GN, Miodownik MA. Acta Mater 2001;49(15):2981–91.
[15] Kazaryan A, Wang Y, Dregia SA, Patton BR. Acta Mater 2002;50(10):2491–502.
[16] Hassold GN, Holm EA, Miodownik MA. Mater Sci Technol 2003;19(6):683–7.
[17] Kinderlehrer D, Livshits I, Rohrer GS, Taasan S, Yu P. In: Recrystallization and Grain Growth, Parts 1 and 2, vols. 467–470, 2004, p. 1063–8.
[18] Gruber J, George DC, Kuprat AP, Rohrer GS, Rollett AD. In B. Bacroix et al. (eds.), Proceedings of the 2nd International Conference on Recrystallization and Grain Growth. Materials Science Forum, vol. 467–470, 2004, p. 733–8.
[19] Barmak K, Archibald WE, Kim J, Kim CS, Rollett AD, Rohrer GS, Taasan S, and Kinderlehrer D. In: ICOTOM 14: Textures of Materials, Parts 1 and 2, vols. 495–497, 2005, p. 1255–60.
[20] Gruber J, George DC, Kuprat AP, Rohrer GS, Rollett AD. Scripta Mater 2005;53(3):351–5.
[21] Gruber J, Rollett AD, Rohrer GS. Acta Mater, in press.
[22] Bunge HJ. Texture analysis in materials science. Boston, MA: Butterworth; 1982.
[23] Rollett AD, Manohar P. In: Raabe D et al., editors. Continuum scale modeling in materials science. Weinheim: Wiley-VCH; 2004.
[24] J Gruber. Thesis, Carnegie Mellon University; 2007.
[25] Read WT, Shockley W. Phys Rev 1950;78(3):275–89.
[26] Hillert M. Acta Metall 1965;13(3):227.
[27] Wakai F, Shinoda Y, Ishihara S, Dominguez-Rodriguez A. J Mater Res 2001;16(7):2136–42.
[28] Rollett AD, Srolovitz DJ, Anderson MP. Acta Metall 1989;37(4):2127.
[29] Holm EA, Miodownik MA, Rollett AD. Acta Mater 2003;51(9):2701–16.